

Nature of the spin resonance mode in CeCoIn₅

Yu Song¹, Weiyi Wang¹, John S. Van Dyke², Naveen Pouse^{3,4}, Sheng Ran^{3,4}, Duygu Yazici^{3,4}, A. Schneidewind⁵, Petr Čermák^{5,7}, Y. Qiu⁶, M. B. Maple^{3,4}, Dirk K. Morr²² & Pengcheng Dai¹

Spin-fluctuation-mediated unconventional superconductivity can emerge at the border of magnetism, featuring a superconducting order parameter that changes sign in momentum space. Detection of such a sign-change is experimentally challenging, since most probes are not phase-sensitive. The observation of a spin resonance mode (SRM) from inelastic neutron scattering is often seen as strong phase-sensitive evidence for a sign-changing superconducting order parameter, by assuming the SRM is a spin-excitonic bound state. Here we show that for the heavy fermion superconductor CeCoIn₅, its SRM defies expectations for a spin-excitonic bound state, and is not a manifestation of sign-changing superconductivity. Instead, the SRM in CeCoIn₅ likely arises from a reduction of damping to a magnon-like mode in the superconducting state, due to its proximity to magnetic quantum criticality. Our findings emphasize the need for more stringent tests of whether SRMs are spin-excitonic, when using their presence to evidence sign-changing superconductivity.

¹Department of Physics and Astronomy, Rice University, Houston, TX 77005, USA. ²Department of Physics, University of Illinois at Chicago, Chicago, IL 60607, USA. ³Department of Physics, University of California, San Diego, La Jolla, CA 92093, USA. ⁴Center for Advanced Nanoscience, University of California, San Diego, La Jolla, CA 92093, USA. ⁵Jülich Center for Neutron Science JCNS, Forschungszentrum Jülich GmbH, Outstation at MLZ, D-85747 Garching, Germany. ⁶NIST center for Neutron Research, National Institute of Standards and Technology, Gaithersburg, MD 20899, USA. ⁷Present address: Department of Condensed Matter Physics, Faculty of Mathematics and Physics, Charles University, Praha, Czech Republic. ✉email: yusong@berkeley.edu; dkmorr@uic.edu; pdai@rice.edu

Understanding the physics of unconventional superconductors, which include cuprate, iron-based, and heavy fermion superconductors, remains a major challenge in condensed matter physics. Unlike conventional superconductors with phonons responsible for binding electrons into pairs, pairing in unconventional superconductors occurs due to electronic interactions^{1–3}. The proximity to magnetically ordered states in these materials suggests spin fluctuations as a common thread that can pair electrons in unconventional superconductors^{3–5}. Unlike phonon-mediated conventional superconductors with superconducting order parameters $\Delta(\mathbf{k})$ that depend weakly on momentum \mathbf{k} , spin-fluctuation-mediated superconductivity requires a $\Delta(\mathbf{k})$ that changes sign in momentum space⁴. Therefore, the experimental determination of whether a sign-change occurs in $\Delta(\mathbf{k})$ is paramount for identifying and testing the spin-fluctuation-mediated pairing mechanism.

While sign-changing superconductivity in cuprate superconductors has been confirmed through phases-sensitive tunneling experiments^{6,7}, such direct experimental evidence is lacking in most other systems where a sign-change has been proposed. Most experimental techniques, including penetration depth, specific heat, thermal conductivity, and angle-resolved photoemission, can probe the magnitude of the superconducting order parameter and its momentum dependence⁷, but are not phase-sensitive. The observation of a spin resonance mode (SRM) in inelastic neutron scattering is commonly regarded as strong phase-sensitive evidence for a sign-changing superconducting order parameter^{4,8–11}, based on the assumption that the SRM is a spin-exciton appearing below the particle-hole continuum onset (PHCO), and at a momentum transfer \mathbf{Q} that connects parts of the Fermi surface exhibiting a sign-change in the superconducting order parameter [$\Delta(\mathbf{k}) = -\Delta(\mathbf{k} + \mathbf{Q})$].

Experimentally, the SRM is typically identified through the appearance of additional magnetic scattering in the superconducting state relative to the normal state, peaking at a well-defined energy E_r and an intensity that tracks the superconducting order parameter⁸. While such behaviors of the SRM are consistent with the spin-exciton scenario, alternative explanations have also been proposed^{8,12–16}. Moreover, phenomenologically similar enhanced scattering in the superconducting state have been observed in systems without sign-changing superconductivity, including phonons^{17,18} and hydrogen tunneling excitations¹⁹ in conventional superconductors and the resonant magnetic exciton mode in semiconducting rare-earth borides^{20,21}, indicating mechanisms other than sign-changing superconductivity that could account for the experimental signatures of the SRM. Therefore, it is important to test whether experimentally observed SRMs are indeed spin-excitonic in nature, given the presence of a SRM is often used to evidence sign-changing unconventional superconductivity. This is underscored by recent measurements on CeCu_2Si_2 that demonstrated it exhibits nodeless superconductivity^{22–25}, despite the observation of a SRM which suggests nodal d -wave superconductivity in the spin-exciton scenario^{26,27}.

In this work, we use inelastic neutron scattering to systematically study the SRM in the prototypical heavy fermion superconductor CeCoIn_5 ($T_c = 2.3$ K)^{28,29}, which exhibits sign-changing $d_{x^2-y^2}$ -wave superconductivity similar to the cuprates^{30–32}. Contrary to expectations for a spin-excitonic SRM with a prominent downward dispersion, our results show that the SRM in CeCoIn_5 disperses upward without downward-dispersing features. Under applied magnetic field, the SRM splits into two upward-dispersing branches, with the dispersive features becoming progressively smeared out due to an increase in damping. Taken together, our results suggest that the SRM in CeCoIn_5 is not spin-excitonic, and therefore is not a

manifestation of the $d_{x^2-y^2}$ -wave superconducting order parameter. Instead, it likely results from the removal of damping to a pre-existing magnetic mode in a more strongly coupled unconventional superconductor. Our findings underscore the importance of more stringent tests to verify the spin-excitonic nature of SRMs, when using their presence to evidence sign-changing unconventional superconductivity.

Results

Dispersion of the SRM in CeCoIn_5 at zero-field. In the spin-exciton scenario, the SRM is a bound state residing below the PHCO with $E(\mathbf{Q}) < \min(|\Delta(\mathbf{k})| + |\Delta(\mathbf{k} + \mathbf{Q})|)$, resulting from a sign-change in the superconducting order parameter^{4,8}. For cuprates with a $d_{x^2-y^2}$ -wave superconducting order parameter, the SRM peaks at the antiferromagnetic wavevector $\mathbf{Q}_{\text{AF}} = (0.5, 0.5)$, which connects hot spots that are close to the antinodal points of the $d_{x^2-y^2}$ -wave superconducting order parameter (Fig. 1a). As the SRM disperses away from \mathbf{Q}_{AF} towards \mathbf{Q}_n , which connects the nodal points of the superconductivity order parameter, the PHCO is progressively pushed towards zero. The reduction of the PHCO away from \mathbf{Q}_{AF} requires a spin-excitonic SRM to exhibit a downward dispersion away from \mathbf{Q}_{AF} , so that it stays below the PHCO. Inelastic neutron scattering measurements of the SRM in hole-doped cuprates demonstrated that it dominantly disperses downwards, consistent with expectations of the spin-exciton picture (Fig. 1b)^{33–38}. For iron pnictide superconductors with isotropic s^{\pm} -wave superconducting gaps, the SRM is also consistent with being a spin-exciton^{4,5}. Here, unlike the cuprates, the PHCO depends weakly on momentum \mathbf{Q} , allowing spin-excitonic SRMs to exhibit upward dispersions, as observed in electron-doped³⁹ and hole-doped compounds⁴⁰.

In the prototypical heavy fermion superconductor CeCoIn_5 , like the cuprates, the superconducting order parameter is $d_{x^2-y^2}$ -wave^{30–32} and the SRM peaks around \mathbf{Q}_{AF} in momentum and $E_r \approx 0.6$ meV in energy¹¹; thus also like the cuprates, the PHCO is gradually suppressed moving from \mathbf{Q}_{AF} towards \mathbf{Q}_n (Fig. 1c and d), resulting in a downward dispersion of the SRM in the spin-exciton scenario (Fig. 1d, see Supplementary Note 1 for details)²⁷. Experimentally, however, the SRM is found to be dominated by a robust upward dispersion for $E \gtrsim E_r$, contrary to expectations in the spin-exciton picture^{41,42}. These upward-dispersing features and the strong L -dependence of the SRM in CeCoIn_5 suggest it is a magnon-like mode, rather than a spin-exciton^{16,41}. While the SRM in CeCoIn_5 is dominated by an upward-dispersing branch for $E \gtrsim E_r$, whether a downward-dispersing branch expected in the spin-exciton scenario also exists for $E < E_r$, remains unclear.

To elucidate whether the SRM in CeCoIn_5 has any downward-dispersing features, we carried out detailed inelastic neutron scattering measurements of the SRM in CeCoIn_5 using PANDA, along the $(H, H, 0.5)$ direction for $E \lesssim E_r \approx 0.6$ meV, with results shown in Fig. 2. The magnetic scattering at $E = 0.375$ meV is weaker in the superconducting state compared to the normal state (Fig. 2a), demonstrating a partial gapping of the magnetic fluctuations at this energy upon entering the superconducting state. With increasing energy, scattering in the superconducting state becomes more intense compared to the normal state (Fig. 2b–f), and the SRM can be clearly identified by such enhanced magnetic scattering. Constant-energy scans along $(H, H, 0.5)$ for $E \geq 0.4$ meV (Fig. 2b–f) clearly reveal two peaks at $\mathbf{Q} = (0.5 \pm \delta, 0.5 \pm \delta, 0.5)$, in good agreement with previous work (see Supplementary Fig. 1 and Supplementary Note 2 for details)⁴². While the magnetic scattering for $E = 0.375$ meV appears to be a single peak, its broad width compared to higher energies suggests the magnetic scattering at this energy also

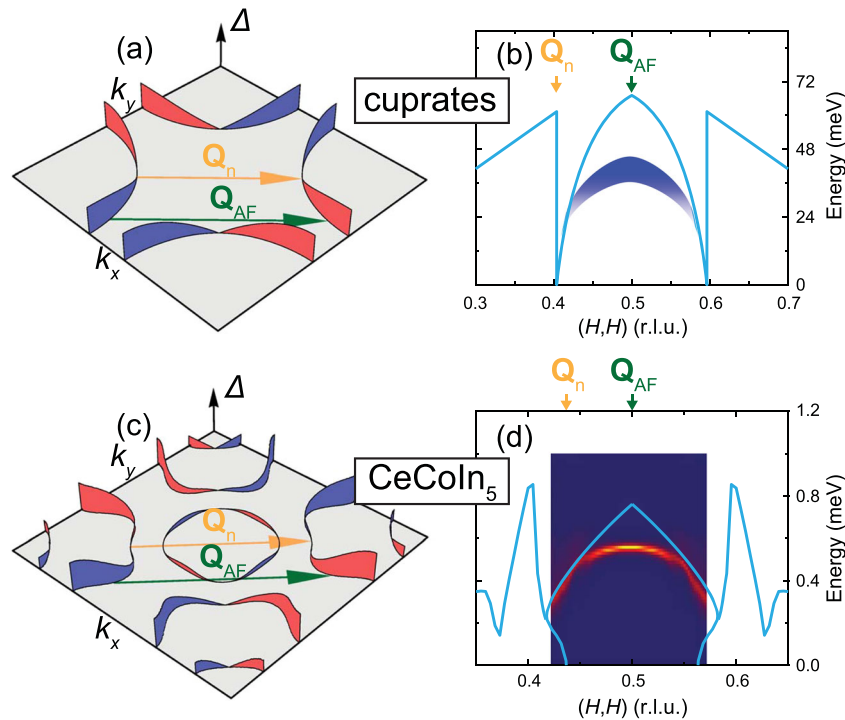


Fig. 1 The spin resonance mode (SRM) in the spin-exciton scenario. **a** Fermi surface and the $d_{x^2-y^2}$ -wave superconducting order parameter in the cuprates⁵⁸. **b** Schematic dispersion of the SRM in the cuprates along the (H, H) direction. The SRM in the cuprates falls below the particle-hole continuum onset (PHCO), indicated by the light blue lines. **c** Fermi surfaces and the $d_{x^2-y^2}$ -wave superconducting order parameter in CeCoIn₅⁴³. **d** Calculated dispersion of the SRM in CeCoIn₅, in the spin-exciton scenario (see Supplementary Note 1 for details). The light blue lines indicate the PHCO. The red and blue surfaces in **a** and **c** represent superconducting order parameters with opposite signs. $\mathbf{Q}_{AF} = (0.5, 0.5)$ connects hot spots on the Fermi surface that exhibits a robust superconducting gap, \mathbf{Q}_n connects parts of the Fermi surface that correspond to nodes of the superconducting order parameter.

consists of two peaks. By fitting the results in Fig. 2b–f using two Gaussian peaks at $\mathbf{Q} = (0.5 \pm \delta, 0.5 \pm \delta, 0.5)$, we find δ does not change significantly for $E \leq 0.45$ meV (Fig. 2b–d) and increases monotonically with increasing energy for $E > 0.45$ meV (Fig. 3a), ruling out any downward-dispersing features. Combined with similar measurements for $E \gtrsim E_r$ obtained using multi-axis crystal spectrometer (MACS) (see Supplementary Figs. 2 and 3 and Supplementary Note 3 for details), we find the SRM in CeCoIn₅ disperses only upward, inconsistent with calculations for the spin-exciton scenario, based on an electronic structure from scanning tunneling microscopy measurements (Figs. 1d and 3a, see Supplementary Note 1 for details)^{31,43}. Instead, the dispersion of the SRM resemble spin waves in CeRhIn₅ (Fig. 3b)^{44,45}, suggesting it to be magnon-like (see Supplementary Fig. 4 and Supplementary Note 2 for additional comparisons).

Splitting of the dispersive SRM under applied magnetic field.

For a spin-excitonic SRM that is isotropic in spin space, the application of a magnetic field should split it into a triplet in energy⁴⁶. In CeCoIn₅, the application of an in-plane magnetic field splits the SRM into a doublet, rather than a triplet^{47,48}, likely due to the presence of magnetic anisotropy^{41,49}. The doublet splitting of the SRM under applied field, combined with the upward dispersion, raises the question of how the dispersive features of the SRM in CeCoIn₅ evolve with applied field, and whether the absence of a downward-dispersing branch is robust under applied field.

To address these questions, we studied the SRM in CeCoIn₅ using MACS, under an applied magnetic field perpendicular to the $[H, H, L]$ scattering plane, with results shown in Figs. 4 and 5. Constant-energy scans along $(H, H, 0.5)$ and $(0.5, 0.5, L)$ directions in Fig. 4 reveal dramatic changes to the SRM away

from \mathbf{Q}_{AF} under applied magnetic field. For $E = 0.5$ meV and $E = 0.6$ meV, the SRM broadens upon increasing the magnetic field from $B = 0$ T to $B = 6$ T (Fig. 4a–d). On the other hand, for $E = 0.8$ meV and $E = 1.0$ meV, two split peaks around \mathbf{Q}_{AF} are clearly seen at $B = 0$ T, while increasing the magnetic field to $B = 3$ T significantly reduces the splitting and only a single peak can be resolved at $B = 6$ T (Fig. 4e–h). We note that while the SRM is peaked slightly away from \mathbf{Q}_{AF} for $E \lesssim E_r$ at zero-field, as demonstrated in Fig. 2, the resolution of our MACS measurements is insufficient to resolve such a small splitting, instead a single peak at \mathbf{Q}_{AF} is observed (Fig. 4a and c).

These disparate behaviors at different energies can be understood to result from the doublet splitting of the upward-dispersing SRM, as schematically depicted in Fig. 4i. The broadening of the peaks along $(H, H, 0.5)$ at $E = 0.5$ and 0.6 meV under applied field is due to a downward shift of the lower branch of the SRM, and increased damping resulting from the PHCO also moving to lower energies. For higher energies $E = 0.8$ and 1.0 meV, the intensity of magnetic scattering is dominated by the upper branch, and because the upper branch moves to higher energies under applied field, a reduction in peak splitting is observed. Our results indicate the dispersive SRM in CeCoIn₅ splits into two branches under an in-plane magnetic field, while maintaining its upward-dispersing character. This conclusion is also supported by the analysis of peak splittings for the data in Fig. 5 (see Supplementary Fig. 5 and Supplementary Note 4 for details).

In addition to splitting the SRM into two upward-dispersing branches, energy- $(H, H, 0.5)$ and energy- $(0.5, 0.5, L)$ maps in Fig. 5 and Supplementary Fig. 6 (obtained from data shown in Supplementary Figs. 3, 7 and 8, see Supplementary Note 3 for details) suggest that applied magnetic field also results in

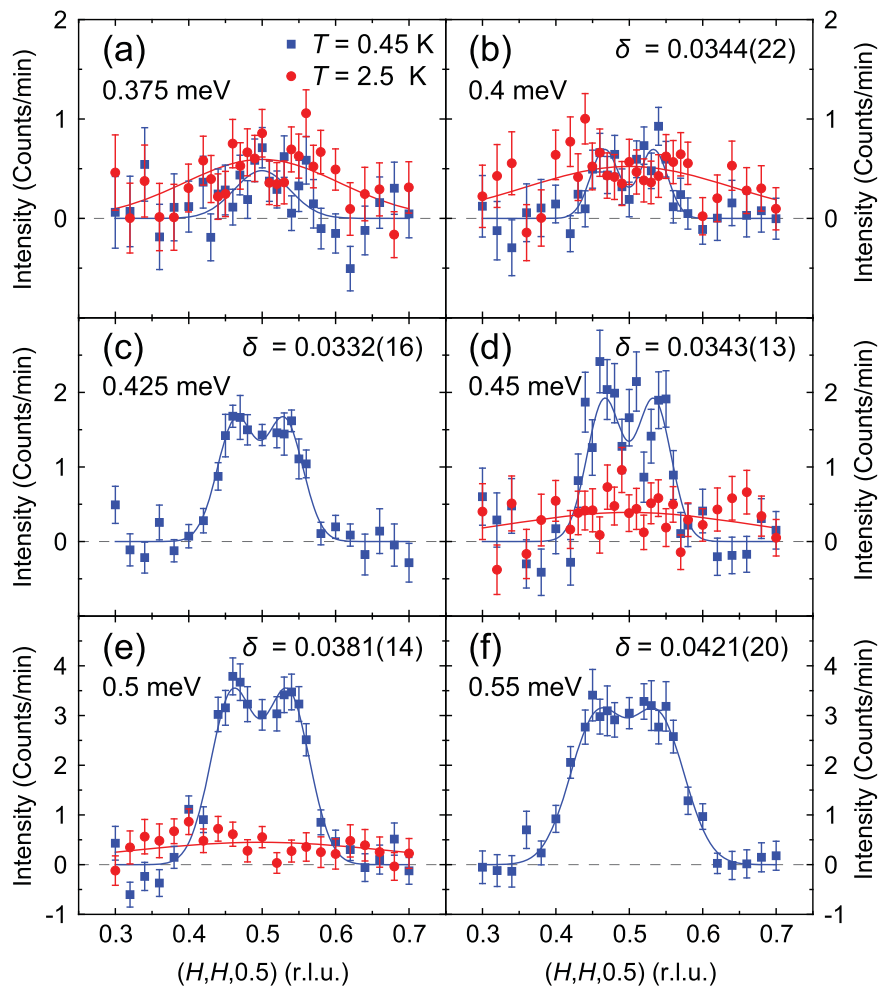


Fig. 2 Constant-energy scans along $(H, H, 0.5)$ for $E \lesssim E_c$. Background-subtracted constant-energy scans measured using PANDA, for **a** $E = 0.375$ meV, **b** $E = 0.4$ meV, **c** $E = 0.425$ meV, **d** $E = 0.45$ meV, **e** $E = 0.5$ meV, and **f** $E = 0.55$ meV. Blues squares are data at $T = 0.45$ K, well below $T_c = 2.3$ K. Red circles are data at $T = 2.5$ K, just above T_c . Solid blue lines are fits to two Gaussian peaks centered at $(0.5 \pm \delta, 0.5 \pm \delta, 0.5)$ for data in the superconducting state, except for $E = 0.375$ meV, which is fit to a single Gaussian peak. Solid red lines are fits to a single Gaussian peak for data in the normal state. A linear background included in the fitting has been subtracted. For panels **b-f**, the fit values and uncertainties of δ are shown in the upper right corner. All vertical error bars in the figures represent statistical errors of 1 s.d.

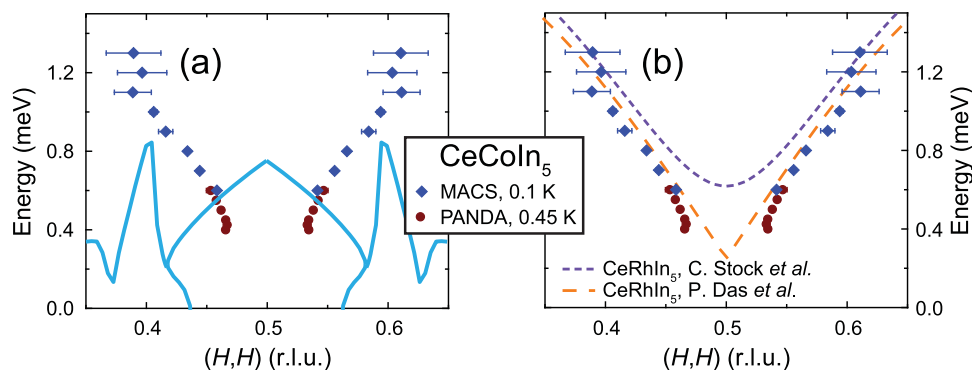


Fig. 3 Zero-field dispersion of the spin resonance mode (SRM). **a** The experimentally observed dispersion of the SRM in CeCoIn₅, compared with the particle-hole continuum onset (PHCO) (light blue lines). **b** The experimentally observed dispersion of the SRM in CeCoIn₅, compared with spin waves in CeRhIn₅^{44,45}. Horizontal error bars are least-square fit errors (1 s.d.), diamond symbols are from multi-axis crystal spectrometer (MACS) data (see Supplementary Note 3 for details) and circle symbols are from PANDA data (Fig. 2).

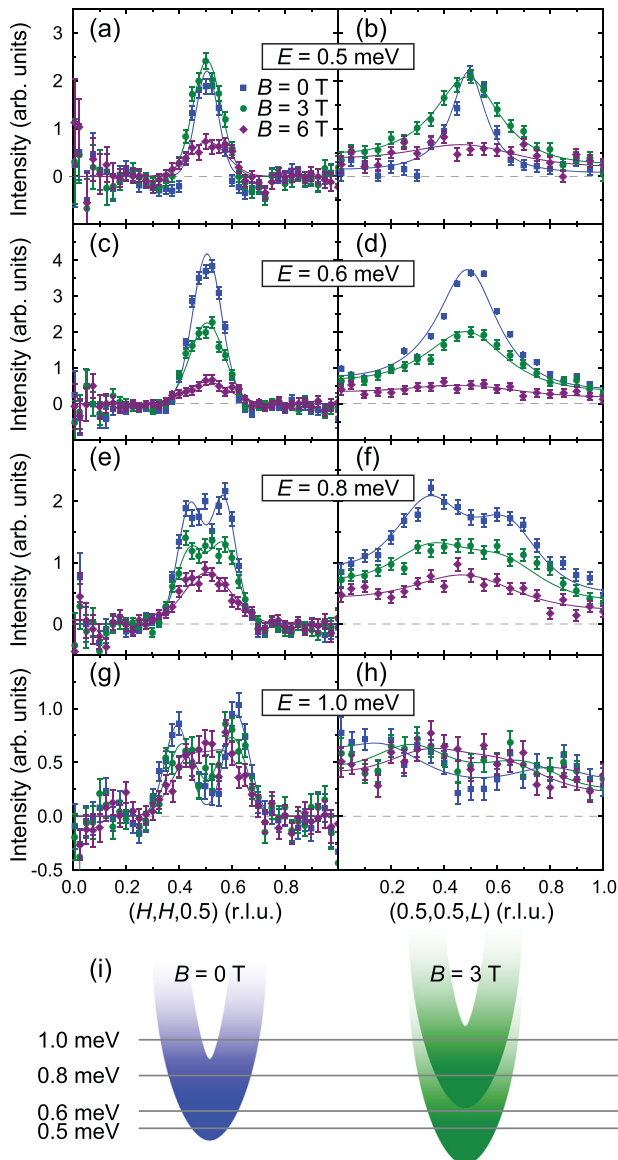


Fig. 4 Constant-energy scans under applied magnetic field. Constant-energy scans along $(H, H, 0.5)$ measured using multi-axis crystal spectrometer (MACS), for **a** $E = 0.5$ meV, **c** $E = 0.6$ meV, **e** $E = 0.8$ meV, and **g** $E = 1.0$ meV, under different applied magnetic fields. Constant-energy scans along $(0.5, 0.5, L)$, for **b** $E = 0.5$ meV, **d** $E = 0.6$ meV, **f** $E = 0.8$ meV, and **h** $E = 1.0$ meV. The normal state magnetic scattering measured at $T = 2.5$ K has been subtracted. For $(H, H, 0.5)$ scans, the solid lines are fits to one or two Gaussian peaks; for $(0.5, 0.5, L)$ scans, the solid lines are fits to a lattice sum of one or two Lorentzian peaks. All vertical error bars in the figure represent statistical errors of 1 s.d. **i** Schematic doublet splitting of the spin resonance mode (SRM) in CeCoIn_5 under applied magnetic field, resulting in two branches that both disperse upward.

significant damping to the SRM in CeCoIn_5 (see Supplementary Fig. 9 and Supplementary Note 4 for additional evidence from constant- Q scans). While the dispersive features can be clearly observed in the $B = 0$ T data (Fig. 5a and b), with applied field the dispersive features become less prominent for $B = 4$ T (Fig. 5c and d) and for $B = 6$ T no dispersive features can be resolved (Supplementary Fig. 6d and h). These results suggest that with applied field, the SRM becomes progressively damped and its dispersive character smeared out, becoming similar to overdamped magnetic excitations in the normal state, as the applied

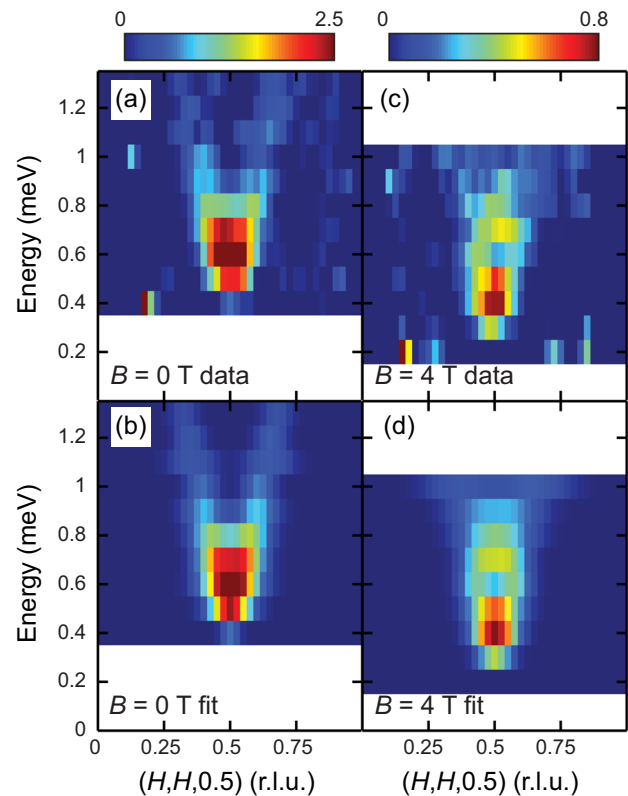


Fig. 5 Energy- $(H, H, 0.5)$ maps under applied magnetic field. Energy- $(H, H, 0.5)$ maps of the spin resonance mode (SRM) in CeCoIn_5 measured using multi-axis crystal spectrometer (MACS), for **a** $B = 0$ T, and **b** $B = 4$ T, with the corresponding fits shown in **c** and **d**, respectively. The normal state magnetic scattering measured at $T = 2.5$ K has been subtracted. $B = 0$ T data are measured with $E_f = 3.7$ meV, and $B = 4$ T data are measured with $E_f = 3.0$ meV. The fits are obtained by combining individual fits to line cuts (see Supplementary Note 3 for details).

field approaches the upper critical field (see Supplementary Fig. 10 and Supplementary Note 3 for details). The increase in damping is unexpected in the spin-exciton scenario. This is because the SRM and the PHCO are shifted in energy in unison by an applied magnetic field, the SRM should therefore remain undamped (see Supplementary Fig. 11 and Supplementary Note 1 for details). Instead, the observed damping of the SRM with increasing field suggests that the SRM and the PHCO move independently with increasing magnetic field, consistent with the suggestion that the SRM in CeCoIn_5 results from the removal of damping to a pre-existing magnetic mode in the superconducting state^{16,41}, rather than being a spin-exciton.

Discussion

Our results demonstrate the SRM in CeCoIn_5 disperses upward, without downward dispersing features, inconsistent with expectations for a spin-exciton in a $d_{x^2-y^2}$ -wave superconductor. This suggests that either the superconducting order parameter in CeCoIn_5 is not $d_{x^2-y^2}$ -wave, or that the SRM is not spin-excitonic. While nodeless s^\pm superconductivity has been proposed for Pu-based 115 heavy-fermion superconductors^{50,51}, there is strong experimental evidence for $d_{x^2-y^2}$ -wave superconductivity in CeCoIn_5 with a robust nodal $d_{x^2-y^2}$ -wave superconducting order parameter^{30-32,41,52}. Therefore, our findings indicate the SRM in CeCoIn_5 is not spin-excitonic in origin, and as such, it is not a manifestation of the sign-changing $d_{x^2-y^2}$ -wave superconducting order parameter in CeCoIn_5 . More broadly, our results highlight

that while SRMs in different unconventional superconductors exhibit similar experimental signatures, they may have distinct origins. When a SRM is spin-excitonic in origin, it evidences sign-changing superconductivity and provides information about the system's electronic structure. On the other hand, if the SRM has a different origin, it may not be appropriate to use the observation of a SRM for these purposes. We note that while a spin-excitonic contribution to the SRM with intensity weaker than our detection limit cannot be ruled out, this does not affect our conclusion that the detectable SRM in CeCoIn₅ is not spin-excitonic.

In the cuprates, X-shaped or Y-shaped excitations with dominant upward dispersing branches, which may result from either localized or itinerant electrons, have been observed^{38,53–57}. However, these upward-dispersing excitations are different from what we have observed in CeCoIn₅ in that they are already present in the normal state, and exhibits little or no change upon entering the superconducting state, i.e. they are not SRMs. When a SRM is present, as seen through additional magnetic scattering uniquely associated with the superconducting state, it is always dominated by a downward dispersion, as shown in Fig. 1b. While a weaker upward-dispersing branch of the SRM has also been detected in some cuprates^{35–37}, these SRMs were shown to be consistent with spin-excitons residing in a different region of momentum space^{35,58}, where the PHCO energy is large (region with $|\mathbf{Q}| < |\mathbf{Q}_n|$ in Fig. 1b). In CeCoIn₅, based on the electronic structure extracted from scanning tunneling microscopy measurements^{31,43}, it can be seen that while a similar region of the PHCO is present (Fig. 3a), it does not account for our experimentally determined dispersion in CeCoIn₅. While the observation of a spin-excitonic SRM indicates sign-changing superconductivity, the absence of a SRM (as seen experimentally in sufficiently underdoped cuprates⁵⁶) or the observed SRM not being spin-excitonic (as in CeCoIn₅) does not invalidate sign-changing superconductivity, but simply means that in these cases information on the superconducting order parameter do not directly manifest in magnetic excitations.

In addition to demonstrating the SRM in CeCoIn₅ disperses upward at zero-field, our results in Fig. 2 also show that the SRM is appropriately described by two peaks at $\mathbf{Q} = (0.5 \pm \delta, 0.5 \pm \delta, 0.5)$ for all energies. The splitting of the SRM for $E < E_r$ is suggested to evidence that the SRM is a precursor^{42,47,59} to the field-induced spin-density-wave phase (Q-phase) that orders at $\mathbf{Q} = (0.5 \pm \delta_Q, 0.5 \pm \delta_Q, 0.5)$ ^{60,61}. For $E \lesssim 0.45$ meV, our data in Fig. 2 shows that $\delta \approx 0.034$, significantly smaller than $\delta_Q = 0.05$. While CeCoIn₅ is magnetically disordered, it can be tuned towards commensurate magnetic order at \mathbf{Q}_{AF} through Cd-doping⁶², Rh-doping⁶³, or Hg-doping⁶⁴, as well as incommensurate magnetic order at $\mathbf{Q} = (0.5 \pm \delta_Q, 0.5 \pm \delta_Q, 0.5)$ through Nd-doping⁶⁵ or applying magnetic field⁶⁰. The proximity of CeCoIn₅ to two types of magnetic orders indicates that fluctuations associated with both may be present in CeCoIn₅, also suggested by two types of fluctuations unveiled by half-polarized neutron scattering experiments⁴⁸. In such a scenario, the overlap of fluctuations at $\mathbf{Q} = (0.5 \pm \delta_Q, 0.5 \pm \delta_Q, 0.5)$ and \mathbf{Q}_{AF} results in the observed $\delta < \delta_Q$ for $E \lesssim E_r$ (see Supplementary Fig. 1 and Supplementary Note 2 for details). Such a coexistence of two types of magnetic fluctuations has also been observed in FeTe^{66,67}; in both CeCoIn₅ and FeTe, it results from the quasi-degeneracy of different magnetic states.

While a SRM that is isotropic in spin space is expected to split into triplets in energy under applied field⁴⁶, when an easy-plane magnetic anisotropy perpendicular to the field direction (110) is taken into consideration, it is possible to account for the doublet splitting in CeCoIn₅^{41,49}. However, the SRM has been demonstrated to have an Ising character at zero-field, with the easy-axis along (001)⁴²; therefore, to account for the doublet splitting of the

SRM in CeCoIn₅, it is necessary to consider modifications to the form of magnetic anisotropy under applied magnetic field, as demonstrated for magnetically ordered CeRhIn₅⁶⁸. At zero-field, CeRhIn₅ exhibits an easy-*ab*-plane spin anisotropy, an applied magnetic field along (110) induces an anomalously large additional easy-axis anisotropy along (110), driving the system to exhibit an easy-axis spin anisotropy along (110) overall. In the case of CeCoIn₅, at zero-field it exhibits an easy-axis spin anisotropy along (001), and if an applied magnetic field along (110) also eases the spin anisotropy along (110) as in CeRhIn₅, the system may be driven to overall exhibit an easy-plane-like spin anisotropy, with the easy-plane spanned by (001) and (110) (perpendicular to the applied field).

In conclusion, our detailed inelastic neutron scattering measurements indicate the SRM in CeCoIn₅ disperses upward without any downward dispersing features, indicating it is not spin-excitonic in origin. Under an applied magnetic field, the SRM splits into two upward-dispersing branches and progressively loses its dispersive characters with increasing field, suggesting the SRM in CeCoIn₅ results from the removal of damping to a pre-existing magnetic mode in the superconducting state. As such, our results suggest the SRM in CeCoIn₅ is not a result of the sign-change in its superconducting order parameter. Our findings demonstrate SRMs observed in unconventional superconductors can have origins other than spin-excitonic, in which case their presence may not provide information on the superconducting order parameter.

Methods

Sample preparation and neutron scattering experimental setups. Single crystals of CeCoIn₅ were prepared by the indium self-flux method⁶⁹. Hundreds of CeCoIn₅ single crystals with a total mass ~1 g were co-aligned in the $[H, H, L]$ scattering plane on aluminum plates using a hydrogen-free glue. Magnetic field is applied perpendicular to the scattering plane, along the (110) direction.

Neutron scattering experiments were carried out on the PANDA cold three-axes spectrometer at the Heinz Maier-Leibnitz Zentrum⁷⁰ and the MACS at the NIST Center for Neutron Research. The inelastic neutron scattering experiments on PANDA used fixed $k_f = 1.3 \text{ \AA}^{-1}$. A sapphire filter is used before the monochromator and a Be filter cooled to 40 K is used before the sample. The monochromator has horizontal and vertical variable focusing mechanics, vertical focusing of the analyzer is fixed (variable focusing is not needed because the detector is a vertically placed 1 inch ³He tube) and horizontal focusing is variable. In the focused mode, variable focusings are adjusted depending on the neutron wavelength based on empirically optimized values. The inelastic neutron scattering measurements at MACS used Be filters both before and after the sample with fixed $E_f = 3.0$ meV or $E_f = 3.7$ meV. Most of measurements on MACS were made using the 20 spectroscopic detectors simultaneously to efficiently obtain the magnetic scattering within the $[H, H, L]$ scattering plane. Constant-Q scans at \mathbf{Q}_{AF} shown in Supplementary Fig. 9 were carried out using MACS with a single detector. The analyzers are vertically focused, while the monochromator is doubly focused.

Data analysis. Data shown in Fig. 2 and Supplementary Fig. 1 are obtained using PANDA. The constant-energy scans were fit to a single Gaussian peak or two Gaussian peaks equally displaced from the center; scans at different energy transfers are fit globally with the same peak center. Constant-Q scans in Supplementary Fig. 9 are measured on MACS using a single detector. All the rest of neutron scattering data are obtained using MACS by measuring maps of large portions of the $[H, H, L]$ scattering plane, simultaneously using the 20 detectors available at MACS. The maps of $[H, H, L]$ -plane are folded into a single quadrant to improve statistics. Cuts along $(H, H, 0.5)$ were obtained by binning data with $0.37 \leq L \leq 0.63$ and a step size of 0.025; cuts along $(0.5, 0.5, L)$ are obtained by binning data with $(0.42, 0.42) \leq (H, H) \leq (0.58, 0.58)$ and a step size of 0.05. Normal state magnetic excitations measured at $T = 2.5$ K have been subtracted in all the MACS data except Supplementary Fig. 10. The cuts along $(H, H, 0.5)$ are fit with a single Gaussian peak centered at $\mathbf{Q} = (0.5, 0.5, 0.5)$ or two Gaussian peaks at $\mathbf{Q} = (0.5 \pm \delta, 0.5 \pm \delta, 0.5)$. The cuts along $(0.5, 0.5, L)$ are fit using a lattice sum of a single Lorentzian peak centered at $\mathbf{Q} = (0.5, 0.5, 0.5)$ or a lattice sum of two Lorentzian peaks at $\mathbf{Q} = (0.5, 0.5, 0.5 \pm \delta)$. $B = 4$ T data are collected using $E_f = 3.0$ meV, while measurements at other fields used $E_f = 3.7$ meV. Using MACS we collected high statistics data for selected energies (Fig. 4 and Supplementary Fig. 2) and lower statistics data with finer energy steps (Fig. 5 and Supplementary Figs. 3, 6–8). The zero-field data shown in Fig. 4 and Supplementary Fig. 2 are reproduced from ref. ⁴¹, to compare with data under applied field.

Data availability

All relevant data are available from the corresponding authors upon reasonable request.

Received: 17 January 2020; Accepted: 4 May 2020;

Published online: 29 May 2020

References

- Norman, M. R. The challenge of unconventional superconductivity. *Science* **332**, 196–200 (2011).
- Stewart, G. R. Unconventional superconductivity. *Adv. Phys.* **66**, 75–196 (2017).
- Keimer, B., Kivelson, S. A., Norman, M. R., Uchida, S. & Zaanen, J. From quantum matter to high-temperature superconductivity in copper oxides. *Nature* **518**, 179–186 (2015).
- Scalapino, D. J. A common thread: the pairing interaction for unconventional superconductors. *Rev. Mod. Phys.* **84**, 1383 (2012).
- Dai, P. C. Antiferromagnetic order and spin dynamics in iron-based superconductors. *Rev. Mod. Phys.* **87**, 855 (2015).
- Van Harlingen, D. J. Phase-sensitive tests of the symmetry of the pairing state in the high-temperature superconductors—evidence for $d_{x^2-y^2}$ symmetry. *Rev. Mod. Phys.* **67**, 515 (1995).
- Tsuei, C. C. & Kirtley, J. R. Pairing symmetry in cuprate superconductors. *Rev. Mod. Phys.* **72**, 969 (2000).
- Eschrig, M. The effect of collective spin-1 excitations on electronic spectra in high- T_c superconductors. *Adv. Phys.* **55**, 47–183 (2006).
- Rossat-Mignod, J. et al. Neutron scattering study of the $\text{YBa}_2\text{Cu}_3\text{O}_{6-x}$ system. *Physica C* **185**, 86–92 (1991).
- Christianson, A. D. et al. Unconventional superconductivity in $\text{Ba}_{0.6}\text{K}_{0.4}\text{Fe}_2\text{As}_2$ from inelastic neutron scattering. *Nature* **456**, 930–932 (2008).
- Stock, C., Broholm, C., Hudis, J., Kang, H. J. & Petrovic, C. Spin resonance in the d -wave superconductor CeCoIn_5 . *Phys. Rev. Lett.* **100**, 087001 (2008).
- Morr, D. K. & Pines, D. The resonance peak in cuprate superconductors. *Phys. Rev. Lett.* **81**, 1086 (1998).
- Krüger, F. et al. Magnetic fluctuations in n -type high- T_c superconductors reveal breakdown of Fermiology: experiments and Fermi-liquid/RPA calculations. *Phys. Rev. B* **76**, 094506 (2007).
- Xu, G. et al. Testing the itinerancy of spin dynamics in superconducting $\text{Bi}_2\text{Sr}_2\text{CaCu}_2\text{O}_{8+\delta}$. *Nat. Phys.* **5**, 642–646 (2009).
- Onari, S., Kontani, H. & Sato, M. Structure of neutron-scattering peaks in both s_{++} -wave and s_x -wave states of an iron pnictide superconductor. *Phys. Rev. B* **81**, 060504 (2010).
- Chubukov, A. V. & Gor'kov, L. P. Spin resonance in three-dimensional superconductors: the case of CeCoIn_5 . *Phys. Rev. Lett.* **101**, 147004 (2008).
- Kawano, H., Yoshizawa, H., Takeya, H. & Kadowaki, K. Anomalous phonon scattering below T_c in $\text{YNi}_2\text{B}_2\text{C}$. *Phys. Rev. Lett.* **77**, 4628 (1996).
- Stassis, C. et al. Phonon mode coupling in superconducting $\text{LuNi}_2\text{B}_2\text{C}$. *Phys. Rev. B* **55**, R8678 (1997).
- Magerl, A., Dianoux, A. J., Wipf, H., Neumaier, K. & Anderson, I. S. Concentration dependence and temperature dependence of hydrogen tunneling in $\text{Nb}(\text{OH})_x$. *Phys. Rev. Lett.* **56**, 159 (1986).
- Friemel, G. et al. Resonant magnetic exciton mode in the heavy-fermion antiferromagnet CeB_6 . *Nat. Commun.* **3**, 830 (2012).
- Nemkovski, K. S., Alekseev, P. A., Mignot, J.-M. & Ivanov, A. S. Resonant mode in rare-earth based strongly correlated semiconductors. *Phys. Proc.* **42**, 18 (2013).
- Yamashita, T. et al. Fully gapped superconductivity with no sign change in the prototypical heavy-fermion CeCu_2Si_2 . *Sci. Adv.* **3**, e1601667 (2017).
- Takenaka, T. et al. Full-gap superconductivity robust against disorder in heavy-fermion CeCu_2Si_2 . *Phys. Rev. Lett.* **119**, 077001 (2017).
- Pang, G. et al. Fully gapped d -wave superconductivity in CeCu_2Si_2 . *Proc. Natl Acad. Sci. USA* **115**, 5343–5347 (2018).
- Li, Y. et al. Gap symmetry of the heavy fermion superconductor CeCu_2Si_2 at ambient pressure. *Phys. Rev. Lett.* **120**, 217001 (2018).
- Stockert, O. et al. Magnetically driven superconductivity in CeCu_2Si_2 . *Nat. Phys.* **7**, 119–124 (2011).
- Eremin, I., Zwicknagl, G., Thalmeier, P. & Fulde, P. Feedback spin resonance in superconducting CeCu_2Si_2 and CeCoIn_5 . *Phys. Rev. Lett.* **101**, 187001 (2008).
- Thompson, J. D. & Fisk, Z. Progress in heavy-fermion superconductivity: Ce115 and related materials. *J. Phys. Soc. Jpn.* **81**, 011002 (2012).
- White, B. D., Thompson, J. D. & Maple, M. B. Unconventional superconductivity in heavy-fermion compounds. *Physica C* **514**, 246–278 (2015).
- Izawa, K. et al. Angular position of nodes in the superconducting gap of quasi-2D heavy-fermion superconductor CeCoIn_5 . *Phys. Rev. Lett.* **87**, 057002 (2001).
- Allan, M. P. et al. Imaging Cooper pairing of heavy fermions in CeCoIn_5 . *Nat. Phys.* **9**, 468–473 (2013).
- Zhou, B. B. et al. Visualizing nodal heavy fermion superconductivity in CeCoIn_5 . *Nat. Phys.* **9**, 474–479 (2013).
- Bourges, P. et al. The spin excitation spectrum in superconducting $\text{YBa}_2\text{Cu}_3\text{O}_{6.85}$. *Science* **288**, 1234–1237 (2000).
- Dai, P. C., Mook, H. A., Hunt, R. D. & Doğan, F. Evolution of the resonance and incommensurate spin fluctuations in superconducting $\text{YBa}_2\text{Cu}_3\text{O}_{6-x}$. *Phys. Rev. B* **63**, 054525 (2001).
- Pailhès, S. et al. Resonant magnetic excitations at high energy in superconducting $\text{YBa}_2\text{Cu}_3\text{O}_{6.85}$. *Phys. Rev. Lett.* **93**, 167001 (2004).
- Reznik, D. et al. Dispersion of magnetic excitations in optimally doped superconducting $\text{YBa}_2\text{Cu}_3\text{O}_{6.95}$. *Phys. Rev. Lett.* **93**, 207003 (2004).
- Hayden, S. M., Mook, H. A., Dai, P. C., Perring, T. G. & Doğan, F. The structure of the high-energy spin excitations in a high-transition-temperature superconductor. *Nature* **429**, 531 (2004).
- Sidis, Y. et al. Inelastic neutron scattering study of spin excitations in the superconducting state of high temperature superconductors. *C. R. Phys.* **8**, 745 (2007).
- Kim, M. G. et al. Magnonlike dispersion of spin resonance in Ni-doped BaFe_2As_2 . *Phys. Rev. Lett.* **110**, 177002 (2013).
- Zhang, R. et al. Neutron spin resonance as a probe of Fermi surface nesting and superconducting gap symmetry in $\text{Ba}_{0.67}\text{K}_{0.33}(\text{Fe}_{1-x}\text{Co}_x)_2\text{As}_2$. *Phys. Rev. B* **98**, 060502 (2018).
- Song, Y. et al. Robust upward dispersion of the neutron spin resonance in the heavy fermion superconductor $\text{Ce}_{1-x}\text{Yb}_x\text{CoIn}_5$. *Nat. Commun.* **7**, 12774 (2016).
- Raymond, S. & Lapertot, G. Ising incommensurate spin resonance of CeCoIn_5 : a dynamical precursor of the Q phase. *Phys. Rev. Lett.* **115**, 037001 (2015).
- Van Dyke, J. S. et al. Direct evidence for a magnetic f -electron-mediated pairing mechanism of heavy-fermion superconductivity in CeCoIn_5 . *Proc. Natl Acad. Sci. USA* **111**, 11663–11667 (2014).
- Das, P. et al. Magnitude of the magnetic exchange interaction in the heavy-fermion antiferromagnet CeRhIn_5 . *Phys. Rev. Lett.* **113**, 246403 (2014).
- Stock, C. et al. Single to multi-quasiparticle excitations in the itinerant helical magnet CeRhIn_5 . *Phys. Rev. Lett.* **114**, 247005 (2015).
- Ismer, J.-P., Eremin, I., Rossi, E. & Morr, D. K. Magnetic resonance in the spin excitation spectrum of electron-doped cuprate superconductors. *Phys. Rev. Lett.* **99**, 047005 (2007).
- Stock, C. et al. Magnetic field splitting of the spin resonance in CeCoIn_5 . *Phys. Rev. Lett.* **109**, 167207 (2012).
- Raymond, S., Kaneko, K., Hiess, A., Steffens, P. & Lapertot, G. Evidence for three fluctuation channels in the spin resonance of the unconventional superconductor CeCoIn_5 . *Phys. Rev. Lett.* **109**, 237210 (2012).
- Akbari, A. & Thalmeier, P. Field-induced spin exciton doublet splitting in $d_{x^2-y^2}$ -wave CeM In_5 ($M = \text{Rh, Ir, Co}$) heavy-electron superconductors. *Phys. Rev. B* **86**, 134516 (2012).
- Ronning, F. et al. Superconducting gap structure of the 115s revisited. *Matter* **24**, 294206 (2012).
- Das, T., Zhu, J.-X. & Graf, M. J. Theory of nodal s^\pm -wave pairing symmetry in the Pu-based 115 superconductor family. *Sci. Rep.* **5**, 8632 (2015).
- Xu, Y. et al. Universal heat conduction in $\text{Ce}_{1-x}\text{Yb}_x\text{CoIn}_5$: evidence for robust nodal d -wave superconducting gap. *Phys. Rev. B* **93**, 064502 (2016).
- Tranquada, J. M. et al. Quantum magnetic excitations from stripes in copper oxide superconductors. *Nature* **429**, 534–538 (2004).
- Fujita, M. et al. Progress in neutron scattering studies of spin excitations in high- T_c cuprates. *J. Phys. Soc. Jpn.* **81**, 011007 (2012).
- Hinkov, V. et al. Spin dynamics in the pseudogap state of a high-temperature superconductor. *Nat. Phys.* **3**, 780–785 (2007).
- Chan, M. K. et al. Commensurate antiferromagnetic excitations as a signature of the pseudogap in the tetragonal high- T_c cuprate $\text{HgBa}_2\text{CuO}_{4+\delta}$. *Nat. Commun.* **7**, 10819 (2016).
- Chan, M. K. et al. Hourglass dispersion and resonance of magnetic excitations in the superconducting state of the single-layer cuprate $\text{HgBa}_2\text{CuO}_{4+\delta}$ near optimal doping. *Phys. Rev. Lett.* **117**, 277002 (2016).
- Eremin, I., Morr, D. K., Chubukov, A. V., Bennemann, K. H. & Norman, M. R. Novel neutron resonance mode in $d_{x^2-y^2}$ -wave superconductors. *Phys. Rev. Lett.* **94**, 147001 (2005).
- Michal, V. P. & Mineev, V. P. Field-induced spin-exciton condensation in the $d_{x^2-y^2}$ -wave superconductor CeCoIn_5 . *Phys. Rev. B* **84**, 052508 (2011).
- Kenzelmann, M. et al. Coupled superconducting and magnetic order in CeCoIn_5 . *Science* **321**, 1652–1654 (2008).
- Gerber, S. et al. Switching of magnetic domains reveals spatially inhomogeneous superconductivity. *Nat. Phys.* **10**, 126–129 (2013).

62. Nicklas, M. et al. Magnetic structure of Cd-doped CeCoIn₅. *Phys. Rev. B* **76**, 052401 (2007).
63. Yokoyama, M. et al. Change of antiferromagnetic structure near a quantum critical point in CeRh_{1-x}Co_xIn₅. *Phys. Rev. B* **77**, 224501 (2008).
64. Stock, C. et al. From ising resonant fluctuations to static uniaxial order in antiferromagnetic and weakly superconducting CeCo(In_{1-x}Hg_x)₅ ($x = 0.01$). *Phys. Rev. Lett.* **121**, 037003 (2018).
65. Raymond, S. et al. Magnetic order in Ce_{0.95}Nd_{0.05}CoIn₅: the Q-phase at zero magnetic field. *J. Phys. Soc. Jpn.* **83**, 013707 (2014).
66. Song, Y. et al. Spin-isotropic continuum of spin excitations in antiferromagnetically ordered Fe_{1.07}Te. *Phys. Rev. B* **97**, 024519 (2018).
67. Tam, D. W. et al. Plaquette instability competing with bicollinear ground state in detwinned FeTe. *Phys. Rev. B* **100**, 054405 (2019).
68. Fobes, D. M. et al. Tunable emergent heterostructures in a prototypical correlated metal. *Nat. Phys.* **14**, 456–460 (2018).
69. Zapf, V. S. et al. Coexistence of superconductivity and antiferromagnetism in CeRh_{1-x}Co_xIn₅. *Phys. Rev. B* **65**, 014506 (2001).
70. Zentrum, H. M. L. et al. PANDA: cold three axes spectrometer. *J. Large-scale Res. Facil.* **1**, A12 (2015).

Acknowledgements

We thank S. Raymond and C. Stock for helpful discussions. The neutron scattering work at Rice is supported by the U.S. DOE, BES under grant no. DE-SC0012311 (P.D.). Part of the material characterization efforts at Rice is supported by the Robert A. Welch Foundation Grant Nos. C-1839 (P.D.). Research at UC San Diego was supported by the US Department of Energy, Office of Basic Energy Sciences, Division of Materials Sciences and Engineering, under Grant No. DEFG02-04-ER46105 (single crystal growth) and US National Science Foundation under Grant No. DMR-1810310 (characterization of physical properties). Access to MACS was provided by the Center for High Resolution Neutron Scattering, a partnership between the National Institute of Standards and Technology and the National Science Foundation under Agreement No. DMR-1508249.

Author contributions

Y.S. and P.D. led the project. The neutron scattering experiments were performed by Y.S., W.W., A.S., P.C., and Y.Q. The samples were prepared by N.P., S.R., D.Y., and M.B.M. Y.

S. co-aligned the samples. Y.S. and W.W. analyzed the data. Theoretical calculations were carried out by J.V.D. and D.K.M. The manuscript was written by Y.S., D.K.M., and P.D. with input from all coauthors.

Competing Interests

The authors declare no competing interests.

Additional information

Supplementary information is available for this paper at <https://doi.org/10.1038/s42005-020-0365-8>.

Correspondence and requests for materials should be addressed to Y.S., D.K.M. or P.D.

Reprints and permission information is available at <http://www.nature.com/reprints>

Publisher's note Springer Nature remains neutral with regard to jurisdictional claims in published maps and institutional affiliations.



Open Access This article is licensed under a Creative Commons Attribution 4.0 International License, which permits use, sharing, adaptation, distribution and reproduction in any medium or format, as long as you give appropriate credit to the original author(s) and the source, provide a link to the Creative Commons license, and indicate if changes were made. The images or other third party material in this article are included in the article's Creative Commons license, unless indicated otherwise in a credit line to the material. If material is not included in the article's Creative Commons license and your intended use is not permitted by statutory regulation or exceeds the permitted use, you will need to obtain permission directly from the copyright holder. To view a copy of this license, visit <http://creativecommons.org/licenses/by/4.0/>.

© The Author(s) 2020